Journal of Multidisciplinary Engineering Science and Technology (JMEST)
ISSN: 2458-9403
Vol. 6 Issue 3, March - 2019

Experimental Investigations Of The Power Quality Of A Photovoltaic/Battery System Supplying An AC Motor Of A Grain Mill

E. Tchoffo Houdji*
Department of Renewable Energies, National Advanced School of Engineering of Maroua, University of Maroua, Maroua, Cameroon.

D. Yamegueu
Laboratory of Renewable Energies and Energy Efficiency, 2iE,
Ouagadougou , Burkina Faso.
Email: dan.yamegueu@gmail.com

M. Kamta
Department of Electrical, Energetic and Automatic Engineering, National Advanced School of Agro Industrial Sciences, University of Ngaoundéré,
Email: martinkamta@gmail.com

Haman-Djalo
Department of Physics, Faculty of Sciences, University of Ngaoundéré, Cameroon.
Email: haman_djalo@yahoo.com

G.J. Kayem
Department of Process Engineering,
National Advanced School of Agro Industrial Sciences,
University of Ngaoundéré, Cameroon.
Email: gjkayem@yahoo.fr

***Corresponding author: tchoffohoudji@gmail.com**

***Abstract*—Running a grain mill powered by a photovoltaic system in a remote area, require the mastery of the power quality of the system. In this paper, the issue of power quality of a PV/battery system supplying an asynchronous motor via an adjustable speed drivel is reported. The asynchronous motor is loaded by a DC generator feeding a resistive load. This DC generator is used to model the mechanical part of a grain mill. The rotation frequency of the AC motor has been controlled by the adjustable speed drive. To carry out these experiments, the inverter of the PV/battery system has been configured so that its output power remains constant even if the irradiance is changing. Thus, the power quality factors have been assessed for different rotation frequencies of AC motor and for different motor load rates. The results have been discussed in accordance with the IEEE standards. Therefore, the motor rotation frequency as well as the motor load rate ranges required for powering a grain mill in remote area by a PV / battery system have been determined with a best accuracy.**

Keywords— power quality; PV/battery system; harmonic distortion rate; adjustable speed drive; grain mill

I. INTRODUCTION

Stand-alone photovoltaic systems still have a bright future, especially in Africa where many countries have taken renewable energy as an approach to meet the dual objective to increase energy access and strengthen low carbon economic resilience [1]. The European Photovoltaic Industry Association estimates for example that between 2013 and 2017, new stand-alone photovoltaic installations will be between 70 and 100MW per year in Africa [2]. For the case of sub-Saharan African countries where the electrification rate is about 35% [3], the interest to develop renewable energies and stand-alone photovoltaic systems, in particular, is well proven. However, photovoltaic sources are intermittent and produce a direct current. Therefore, to power AC loads with such energy sources, it is necessary to use static DC / AC converters which are sources of harmonic distortions [4]. Such power systems are not also well suitable to power asynchronous electric motors due to their large starting current which is about 5 to 6 times the rated current [5]. Thus, storage batteries are often used in this case to make such power systems permanent. Due to the high starting current values of the motors, there is a risk of instantaneous discharge of these batteries at start-up and therefore their premature deterioration. Using an adjustable speed drive (ASD) for a soft start can limit the inrush current to values between 1 and 1.5 times the rated motor current. In fact, the vector and scalar control techniques of asynchronous motors, implemented via ASDs, contribute to improve the performance of these motors in photovoltaic systems, in particular by limiting the large starting currents [6, 7]. The life time of the equipment is thus extended.

Grain mills are systems in which the load varies during operation. Thus, their motors do not operate under the nominal conditions; this leads to additional energy losses [8].To avoid or to minimize

these energy losses, the motor speed should vary regularly to fit the new load [9]. In industry, the adjustable speed drives (ASD) are used to adapt the speed of the motor to its load [10]. They are also used to maintain the motor speed at a constant level when the load is changing [10, 11] or when the motor is operating under partial load conditions. This offers the possibility of reducing the energy consumed by the motor by 30 to 60% [12]. However, due to the topology of their power converters, the ASDs generate and introduce current and voltage harmonic distortions into the system [13]. The order and amplitude of these harmonic distortions depend on the technology of the ASDs and their operating mode [4, 14]. It has been reported that power inverters interfacing photovoltaic arrays to AC loads also produce additional harmonic currents and eventually increase the total harmonic distortion (THD) at the point of common coupling [15 - 17], whereas the degradation of power quality in the system with regard to harmonics is mostly because of the type of load [18].

One can, therefore, carry out an experimental study of the quality of the electrical energy of a stand-alone photovoltaic system supplying an asynchronous motor of a grain mill, controlled via an ASD. The goal is to find the conditions under which the harmonic disturbances injected into the system are within the limits allowed by the IEEE standards [14], or determine the characteristics of the harmonic filters that should be used to eliminate or reduce these harmonic distortions. In the present work, the behavior of an asynchronous motor powered by a stand-alone photovoltaic system will be assessed for different motor load rates and different rotation frequencies fixed by an ASD. In order to achieve this goal, the electrical power parameters of the asynchronous motor as well as the total harmonic distortions of the current and voltage will be measured and discussed with the IEEE standards.

II. MODELLING OF THE GRAIN MILL

The grain mills used in sub-Saharan countries are mainly of two types; namely the grindstone mills and the hammer mills [19 - 21]. They are either powered by thermal or electric motors. In the grindstone mills, the grinding chamber is feed at constant flow rate. They are classified as constant torque rotation systems and thus be modelled by a constant torque. In this category, the motor speed does not change significantly. The active power of the motor is proportional to the required torque and the speed of the motor. In most hammer mills, the grinding chamber is usually fed at a variable flow rate. They are therefore classified as variable torque rotation systems for which the active power of the motor is proportional to the cube of the motor speed [10]. Thus, to study the behavior of these mills, we can study the operation of their motors at various load rates. The schematic diagram to measure the mechanical torque of a motor from a DC generator is given in Fig. 1. Where DCG is the Direct Current Generator and A.P. are the Auxiliaries Poles of the generator.

The motor load rates can be fixed by using a dynamo-generator containing a shunt-excited DC generator. This DC generator stand in for the mechanical part of the grain mill. It is a DC machine with its stator mounted on the ball bearings. It is provided with two lever arms, one of which has a mobile mass of weight P. When its shaft is coupled to that of an asynchronous motor, the equilibrium of its arm using the counterweight allows to assess the mechanical torque developed by the asynchronous motor. The mechanical torque (C) corresponding to an equilibrium position (d) is assessed as in (1):

$$C = P.d \tag{1}$$

Since the experiments are done at constant torque, the rated active power (P_n) of the motor is proportional to its rated speed (N_n) and to its rated mechanical torque (C_n). This power is assessed as in (2).

$$P_n = 2\pi.N_n.C_n \tag{2}$$

The rated mechanical torque and the motor load rate ($\%C_n$) are assessed by (3) and (4) respectively.

$$C_n = \frac{P_n}{2\pi.N_n} \tag{3}$$

$$\%C_n = \frac{C}{C_n} \tag{4}$$

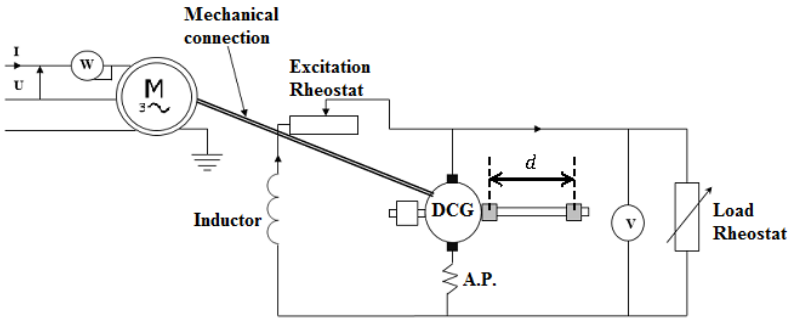

Fig. 1. *Schematic diagram to measure the mechanical torque of a motor from a DC generator*

III. MATERIAL AND METHODS

A. Material

The experimental equipments used for the study are listed in Table 1.

TABLE I. EXPERIMENTAL EQUIPMENTS

Equipments	Rating
Photovoltaic plant	7.35kWp
Park of lead-acid battery	3600Ah
Inverter/charger (Xtender XTH 6000-48)	5kVA
Grid-inverter (SMA STP 8000TL-10)	5kVA
Three-phase ASD (ATV32HU55N4)	5.5kW, 400V
Three-phase wound-rotor Asynchronous motor (LeRoy SOMER, type: NVA132A3)	4.5kW, 400V, 14A, 1395 rpm cos Phi 0.76
Shunt-excited DC generator (LeRoy SOMER, type: LSC132MC7)	3kW, 1500rpm
Resistive load bench	4kW

B. Methodology

Equipments listed in table I are put together to form the experimental set up as shown in Fig. 2. The system studied consists of two energy sources (the photovoltaic plant and the park of solar batteries) and a single load (the controlled motor with its load). So, the power supplied by the photovoltaic plant (P_{PV}) was assessed from the active power of the controlled motor (P_{load}) and the power of the park of solar batteries through the inverter/charger ($P_{battery}$) as given in (5).

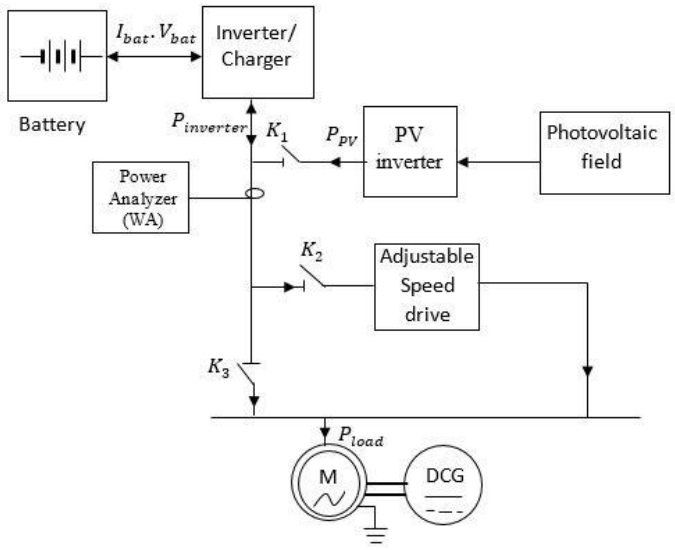

Fig. 2. *Experimental setup diagram*

$$P_{battery} = P_{inverter} = V_{bat}.I_{bat}.\eta_{inverter} \quad (5)$$

Where $\eta_{inverter}$ is the efficiency of the inverter/charger. It was taken equal to 0.96 as given in the datasheet of the inverter. So the contribution of the photovoltaic plant according to Fig. 2 is giving by (6).

$$P_{PV} = P_{load} - P_{battery} \quad (6)$$

The PV/battery system used in this study is such that the PV generator is the main energy source and the battery the secondary one. This battery system behaves as a backup source to fill the power gaps due to the fluctuations of the irradiance. Indeed, the energy produces by the PV plant must be consumed mainly in real time. It is therefore not ideal to pass through the batteries to inject it on the AC bus as in the common stand-alone PV/ battery systems [22]. In this regard, a direct connection of the PV plant to the AC bus through PV inverters is necessary as indicated in Fig. 2. The inverter/charger used is thus able to monitor the charging and discharging of the battery as well as the power flows through the AC bus. In addition to the inverter and battery charger functions available in conventional inverters/chargers, the one used in this work has two specific functions to manage power flows between the PV plant, the battery and the loads. They are *Smart-Boost* and *Frequency Shift Power Control* functions. Thus, if the loads connected to the PV/battery system need more current than that the PV plant can deliver, the batteries will then discharge to provide the surplus if the Smart Boost feature is enabled. The connexion of the PV plant on the AC bus via the PV inverter enables to power the load and to charge the battery via the inverter/charger simultaneously if the production of the PV plant is greater than the needs of the load. However, to avoid the overcharging of the battery with the power from the PV plant, regulation is necessary. This regulation is achieved through the *frequency shift power control* function [23].

Once all these features are enabled in the inverter/charger, five operating modes of the system are possible depending on the state of charge of the battery and the level of irradiance and therefore the contribution of the PV generator to the power absorbed by the load. Let $V_{bat\,min}$ and $V_{bat\,max}$ be the minimum and maximum regulation voltage of the battery respectively.

Mode N° 1 : $P_{PV} \geq P_{load}$ *and* $V_{bat} = V_{bat\,max}$

The battery is fully charged and can't store the excess of energy produced by the photovoltaic plant. The *Frequency Shift Power Control* function of the inverter/charger is used to reduce the power produced by the PV inverter in order to properly feed the load. The battery is in standby.

$$P_{load} \approx P_{PV} \quad (7)$$

Mode N°2 : $P_{PV} > P_{load}$, and $V_{bat\,min} < V_{bat} < V_{bat\,max}$

The *Smart-Boost* function of the inverter/charger is used to allow the battery to be charged. So, the photovoltaic plant powers the load and the battery at the same time.

$$P_{load} = P_{PV} - |P_{battery}| \quad (8)$$

Mode N° 3: $P_{PV} \cong P_{load}$, and $V_{bat\,min} < V_{bat} < V_{bat\,max}$

The *Smart-Boost* function of the inverter/charger is used to allow the battery to be in standby. So, the photovoltaic plant powers the load.

$$P_{load} \cong P_{PV} \quad (9)$$

Mode N° 4 : $P_{PV} < P_{load}$, and $V_{bat\,min} < V_{bat} < V_{bat\,max}$

The *Smart-Boost* function of the inverter/charger is used to allow the battery to be discharged. So, the photovoltaic plant and the battery supply the load simultaneously.

$$P_{load} = P_{PV} + P_{battery} \quad (10)$$

Mode N° 5 : $P_{PV} \approx 0$ and $V_{bat\,min} < V_{bat} < V_{bat\,max}$

This is the operating condition where the sky of the experimental site is shaded. The *Smart-Boost* function of the inverter/charger is used to allow the battery to be discharged. The battery powers the load.

$$P_{load} = P_{battery} = V_{bat}.I_{bat}.\eta_{inverter} \quad (11)$$

It should be noted that in PV systems using batteries as a management storage system, the mode where $V_{bat} < V_{bat\,min}$ is excluded from the sizing of the storage system. Their capacities must satisfy about 5 to 10 times the average daily consumption of the load. The depth of discharge of the battery will be limited and its lifetime will be prolonged [24].

For tests on the motor without photovoltaic plant contribution if needed, the breaker K_1 was opened. For tests on the motor controlled trough the adjustable speed drive (ASD), the breaker K_2 was closed and the breaker K_3 was opened. For tests on the motor without control, the breaker K_2 was opened and the breaker K_3 was closed. A power analyzer (WA) was used and connected as indicated in Fig. 2. For tests with ASD, the considered motor rotation frequencies vary between 40Hz to 55Hz with a step of 5Hz. The scalar control have been implemented for these frequencies. The variation of the motor load ratio was done by changing the values of the resistive load fed by the DC generator. The chosen motor load rates are around 25%; 40%; 50%;60%; 75%; 85%; 100% and 105% (for slight motor overload) of the rated motor torque (C_n).

C. *Instrumentation and electric parameters measured*

During the experiments, the following electric and mechanical characteristics are assessed: the speed of the motor; the torque of the motor; the active (*P*) and reactive (*Q*) powers; the voltage and current total harmonic distortions rates (THD_U and THD_I); the power supply frequency (f) and the power factor (*PF*). These characteristics are obtained using the model C.A 8335 (Qualistar +) power analyser from Chauvin Arnoux [25], connected at the Point of Common Coupling (PCC) of a three phase PV / battery system supplying the nonlinear load. The data were recorded every second and the average values of each parameters on the duration of the test are used in this study. The motor speed was measured using a tachometer. The motor torque was determined from a dynamo-generator containing a shunt-excited DC generator (DCG) feeding a resistive load. Data concerning electric battery parameters were recorded through a data acquisition system included in the monitoring system of the inverter/charger. The irradiance was measured through a meteorological station with a pyranometer (CM 11 pyranometer).

IV. RESULTS AND DISCUSSION

A. *Compensation of the power hollows of the photovoltaic plant*

The graphs displayed in Fig. 3 show an example of the variations of the power flow between the battery ($P_{battery}$), the photovoltaic plant (P_{PV}) and the controlled motor (P_{load}) for different tests done during the day of July 28th, 2016. Tests were carried out for the nominal conditions of the motor (50Hz and 100% of load rate). Except for the operating modes N° 1 and 5, the three others operating modes of the system are exhibited on these graphs. Fig. 3-a shows zones corresponding to the mode No. 3 of operation of the inverter / charger. In this case, the inverter / charger operates in the direction of solar batteries to load. Figs. 3-b and 3-c exhibit zones corresponding to the modes No. 2 and No. 3 of operation of the inverter / charger. In this case, the inverter / charger operates in reversible maner. Fig. 3-d presents zones corresponding to the mode No. 4 of operation of the inverter / charger. In this case, the inverter / charger mainly operates in the direction of solar batteries to load. These figures show that in the variable weather conditions characteristic of tropical climate, a programming Inverter / Charger will automatically compensates the power hollows of a photovoltaic plant. Thus, the PV system / battery / inverter / charger behaves as a permanent electrical power source independently of changes in irradiance.

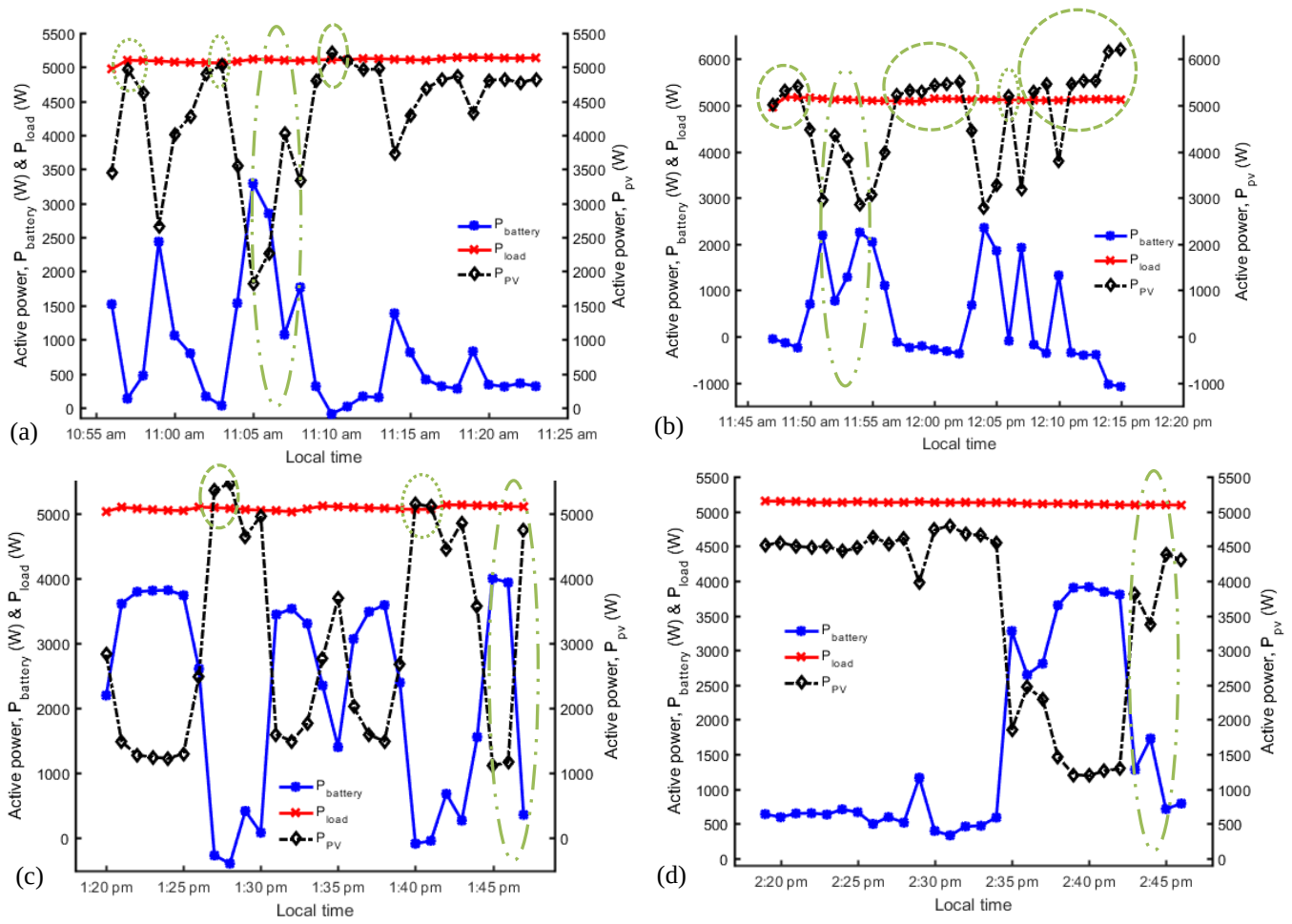

Legend:

: $P_{PV} > P_{load}$; $P_{PV} = P_{load} - P_{battery}$: the battery is charging. This correspond to Mode N° 2.

: $P_{PV} \approx P_{load}$: the battery is in standby. This correspond to Mode N° 3

: $P_{PV} < P_{load}$; $P_{load} = P_{PV} + P_{battery}$; the battery is discharging. This correspond to Mode N° 4.

Fig. 3. *Plots of the energy sources output powers and load power as a function of time on July 28th, 2016*

B. Assessment of power quality factors

1) Total harmonic distortions of current

The variations of the total harmonic distortions of current (THD_I) absorbed by the motor when it is directly connected to the photovoltaic system (motor without control) and generated by the ASD controlling the motor with a scalar control, as a function of the motor load ratio and motor rotation frequency, are shown in Figs. 4 and 5 respectively. From the Fig. 4, it can be seen that the THD_I absorbed by the uncontrolled motor decrease from about 1.6% for low motor loads (less than 50% of rated value) to about 0.89% for nominal load. Thus an asynchronous motor powered by a stand-alone photovoltaic system with battery exhibits low harmonics distortions of current. It is therefore possible to use such a non-linear load in photovoltaic system without adding any harmonic filters since the total harmonic distortions of current is less than that permits by the IEEE 519-1992 standard [14], according to which the THD_I must be less than 5%. However, since the asynchronous motor for a grain mill is used to operate at variable load rates, the use of an ASD is required for ensuring a good dynamic operation of the motor by adapting its power supply to the load and thus reducing the power losses caused by the variation of torque at rated speed [8, 10]. Fig. 4 also shows that the ASD controlling the motor generates harmonic distortions of the current of high amplitudes. The THD_I generated decreases when the motor load ratio increases, with a minimum of about 38% at full load for a motor rotation frequency of 50Hz.

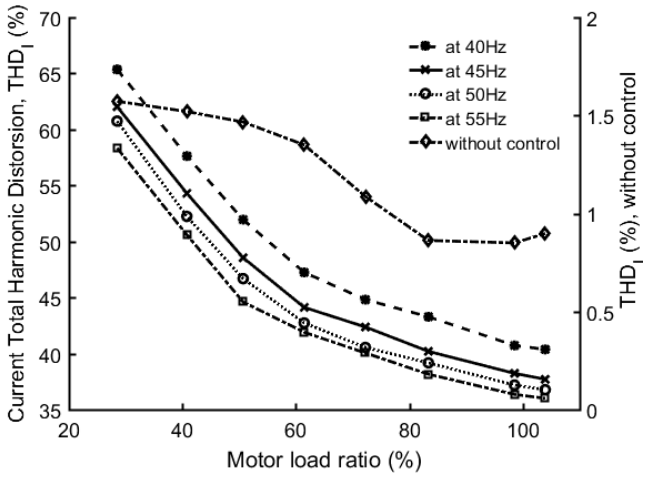

Fig. 4. *Total harmonic distortions of current versus motor load rate at different rotation frequencies*

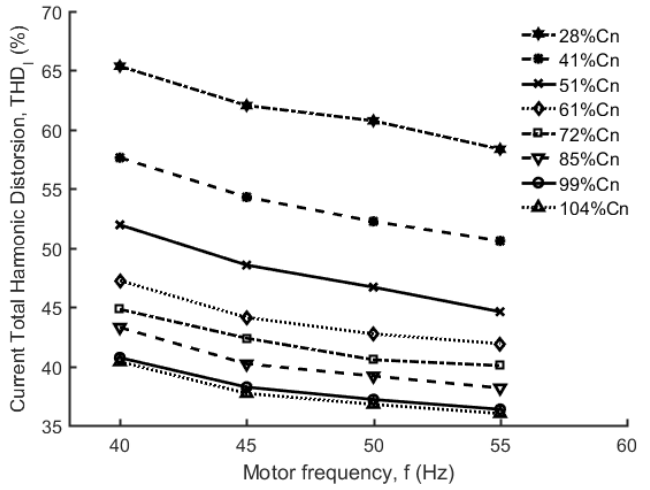

Fig. 5. *Total harmonic distortions of current versus rotation frequency at different motor load rates*

Furthermore, as shown in Fig. 5, for a given motor load ratio, the THD_I generated by the ASD decreases as the motor rotation frequency increases. With the high amplitudes of harmonic distortions of current in this system mainly for low motor loads, the use of a harmonic filter between the PV system and the ASD to bring their values into the recommended range is necessary. Since at low motor load, the active power of the controlled motor is also low (see Figs. 8 and 9), the choice of a sufficiently powerful filter is necessary to take full advantage of the energy saving that can be achieved at these motor loads.

2) Total harmonic distortions of voltage

Figs. 6 and 7 represents the variations of the total harmonic distortions of voltage (THD_U) exhibited by the motor when it is directly connected to the photovoltaic system (motor without control) and generated by the adjustable speed drive (ASD) controlling the motor with a scalar control, as a function of the motor load ratio and motor rotation frequency respectively.

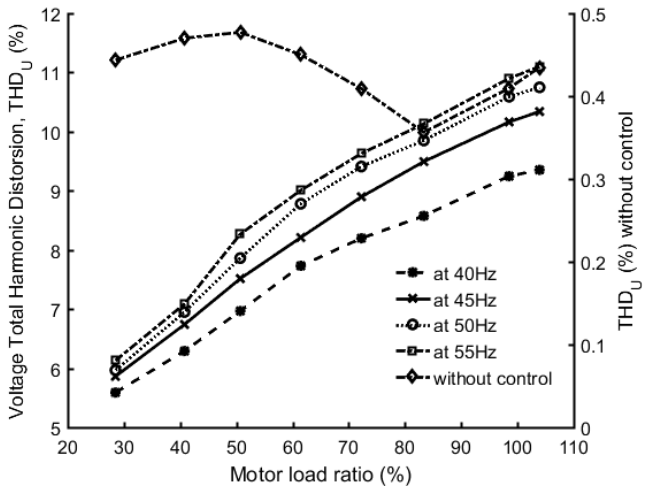

Fig. 6. *Total harmonic distortions of voltage versus motor load rate at different rotation frequencies*

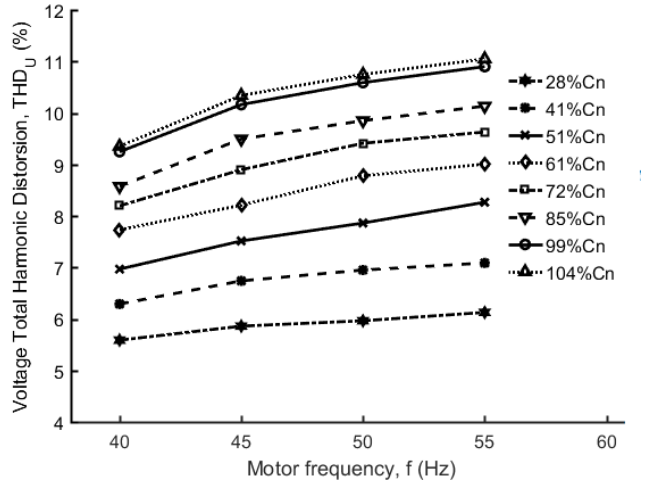

Fig. 7. *Total harmonic distortions of voltage versus rotation frequency at different motor load rates*

The THD_U exhibited by the uncontrolled motor are in the range of 0.35% to 0.48% whatever the load motor rates considered. This trend was expected in view of the variations of the THD_I mentioned above. It can be seen from Fig. 6 that the amplitudes of voltage harmonics distortions generated by the ASD which commands the motor are relatively high. The THD_U increases when the motor load ratio increases, with values of 10.9% at full load for a motor rotation frequency of 50Hz. This is due to the fact that the higher the motor load rate, the more the motor controlled by an ASD absorbs current. Unlike to the case of THD_I, for a given motor load ratio as shown in Fig. 7, the THD_U generated by the ASD increases as the motor rotation frequency increases. This is also due to the fact that, when the motor rotation frequency increases, its voltage also increases and consequently the absorbed current. Referring to IEEE 519-1992 Standard [14], according to which the THD_U must be less than 5% for a grid voltage below 69 kV as in our case, one can conclude that the standard is not respected automatically for the considered motor rotation frequencies. The IEEE 519-

2014 standard [26] specifies other grid voltage ranges, which allows to bring back the range of voltages less than 1.0 kV which is more suitable to our situation. This standard sets the permissible THD_U rate to be less than 8%. Under this standard, for the motor rotation frequency above 50Hz, the controlled motor doesn't meet the standard if the motor load rate is greater than 50%. It is worth noted that these voltage harmonic distortions generated by the ASD are mainly due to the form of the voltages applied to the motor terminals. These are non-sinusoidal voltages produced by the inverter of the ASD. A suitable choice of the control signals frequency of the power transistors of this inverter, their type and even their number can contribute to reduce this voltage harmonic distortion, consequently that of current [27, 28].

3) Active power consumed by the AC motor

The variations of the active power of the controlled motor as a function of the motor load ratio and motor rotation frequency are shown on the Figs. 8 and 9 respectively.

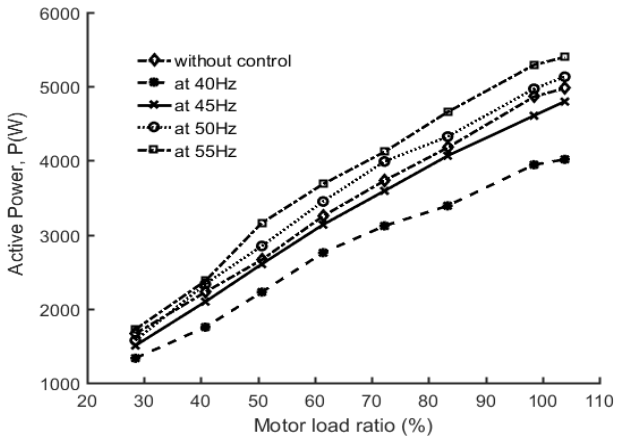

Fig. 8. *Active power versus motor load rate at different rotation frequencies*

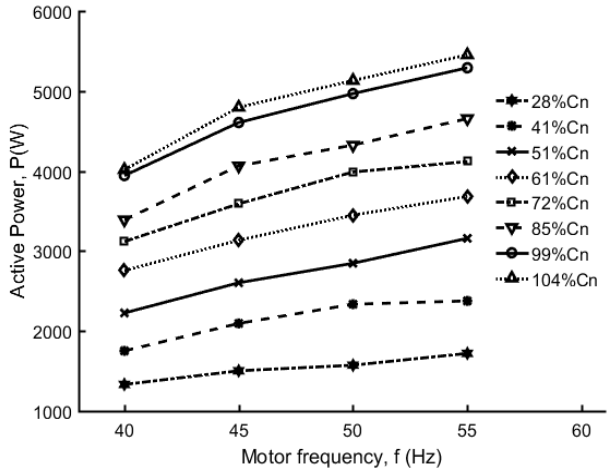

Fig. 9. *Active power versus motor rotation frequency at different motor load rates*

It is shown in Fig. 8 that, for a given rotation frequency of the AC motor, the active power of the controlled motor increase linearly with the motor load ratio. This behavior is inherent to the nature of the motor load. The active power absorbed by the uncontrolled motor and powered at a rotation frequency of 50 Hz is slightly less than that absorbed by the controlled motor at the same rotation frequency. This is due to the extra active power absorbed by the ASD. For a given motor load ratio, the active power absorbed by the controlled motor increases linearly with the rotation frequency as displayed in Fig. 9. The higher the motor load, the steeper the slopes of these lines. It is important to highlight that, for low active powers corresponding to low motor loads, the THD_I are high, reaching about 67% for a motor rotation frequency of 40Hz. This can be explained by the fact that, the inverter operates far below its nominal operating conditions generating strongly deformed current waveforms [29].

4) Reactive power consumed by the AC motor

The variations of the reactive power of the motor as a function of the motor load ratio and motor rotation frequency are shown in Figs. 10 and 11 respectively. From Fig. 10, it is observed that the reactive power absorbed by the uncontrolled motor and powered at a rotation frequency of 50 Hz is very high than that absorbed by the controlled motor in the range of considered rotation frequency. The use of the ASD in this system contributes thus to compensate the reactive power provided by the photovoltaic system, as it is done by FACTS (Flexible Alternating Current Transmission System) devices in any distribution network to improve power quality [30 - 32]. However, it can be seen that the reactive power is negative for motor load rates less than 58% and 50% respectively at 40Hz and 45Hz, while the same behavior is observed for motor load rate less than 45% at frequencies ranged from 50Hz to 55Hz. This indicates the motor load rates limits for which the reactive power is absorbed or supplied by the controlled motor coupled to a DCG. This behavior can be well appreciated in Fig. 11. For motor load rate less than 41%, the reactive power is negative irrespective of the rotation frequency; therefore the controlled motor provides reactive power to the PV system. The controlled motor behaves for these loads rates as a capacitive load. For a motor load rates higher than 60%, the reactive power is positive irrespective of the rotation frequency; the controlled motor absorbs reactive power from the PV power system. In the case where the motor load ratio is about 50%, the reactive power is negative when the motor rotation frequency is less than 45Hz. Above this motor load ratio, the reactive power is positive for the considered range of motor rotation frequencies. The negative reactive powers correspond to the values of THD_I greater than about 48%.

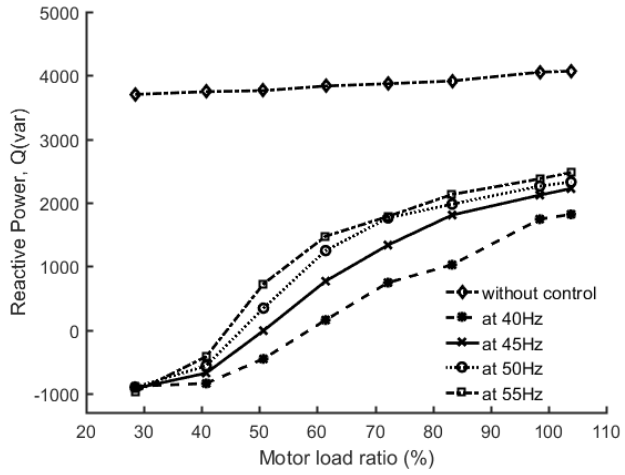

Fig. 10. *Reactive power versus motor load rate at different rotation frequencies*

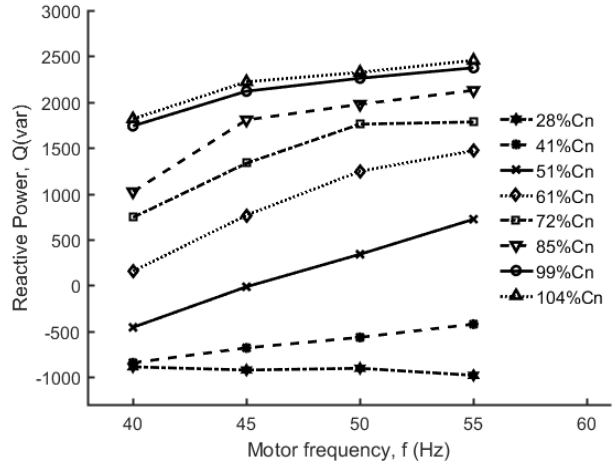

Fig. 11. *Reactive power versus motor rotation frequency at different motor load rates*

Finally, the appropriate motor rotation frequency and load rate ranges for which the PV / battery system can be used to power a controlled motor without provide reactive power to the power system correspond to frequencies greater than 45 Hz and the motor load rate greater than 50%. For the grindstone mills, this corresponds to rotation speeds greater than 1400 rpm, and for hammer mills, to rotation speeds greater than 2800 rpm.

5) Power factor

The variations of the power factor of the ASD system as a function of the motor load ratio are shown on Fig. 12. The power factor of this system is raised compared to the case where the motor is directly connected to the power supply. For this last case, the power factor varies from 0.4 to 0.77 and when the motor is powered through the ASD for the same load ranges, it is between 0.8 and 0.92. The ASD thus contributes to improving the power factor of the system in excellent agreement with [9]. Generally the power quality of the power system is improved as observed with the reduction of the reactive power when the ASD is used to drive the motor.

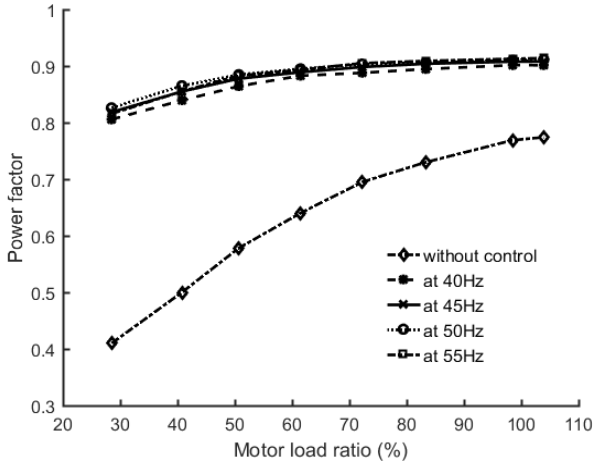

Fig. 12. *Power factor versus motor load rate at different rotation frequencies*

The behavior of the power factor of the ASD system with the variations of the motor rotation frequency is affected by the motor load ratio as shown in Fig. 13. It can be observed from this figure that for motor load rates lower than 61%, the variation of power factor with rotation frequency shows a maximum value at 50 Hz. For motor load rates higher than 61%, this variation is linear. When the motor is loaded near its rate value, the power factor is greater than 0.9 irrespective of the motor rotation frequency. One can also observe that for motor load rate higher than 60%, and the rotation frequency greater than or equal to 50Hz, the power factor seem to be constant.

It is well known that in electrical systems with non-linear loads, the power factor value has to be greater than or equal to 0.9. It can then be concluded that for the system studied in this work, this range corresponds to the motor load rates greater than 60% and rotation frequencies above 45Hz.

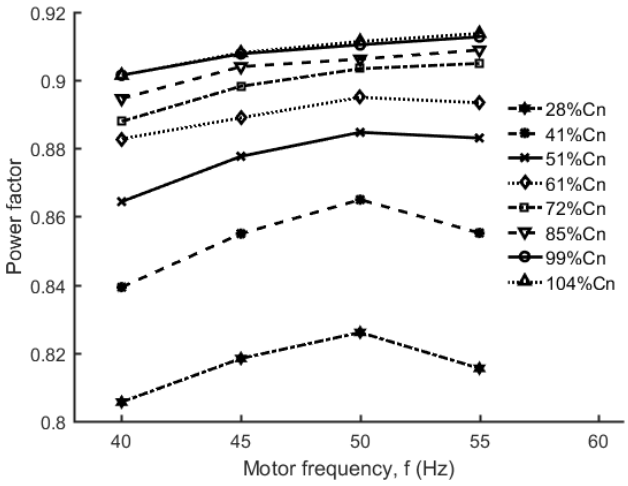

Fig. 13. *Power factor versus motor rotation frequency at different motor load rates*

V. CONCLUSION

In this work, the power quality of a stand-alone photovoltaic system feeding a controlled asynchronous motor for a grain mill has been addressed through experiments. It has been observed that, in the considered ranges of rotation frequency and motor load rate, the non-controlled motor complies with the IEEE 519-1992 standard for harmonic distortion of voltage and current. In these ranges of rotation frequencies and motor load, the controlled motor does not meet this standard for harmonic distortion of current. It meets the standard on voltage harmonic distortion for frequencies below or equal to 50Hz at motor load rates less than 50%.

Another observation is that for the motor load ratio of about 50%, the reactive power of the controlled motor is negative when the rotation frequency is less than 45Hz; the system then behaves as a capacitive load. Thus the controlled motor provides reactive energy to the photovoltaic system for these motor load rates and rotation frequencies. This contributes more to generate harmonic distortions in the system and negatively affects the PV / battery system.

In addition, it has been observed that the power factor of the system varies from 0.8 to 0.9 when the motor is powered through the ASD while it varies from 0.4 to 0.77 when it is directly connected to the PV system for considered motor load rates. It is greater than or equal to 0.9 for load rates greater than 60% and rotation frequencies greater than 45 Hz

Although the use of a harmonic distortion filter is still required, the rotation frequency and motor load rate ranges of [45Hz; 55Hz] and [60%; 100%] are respectively those in which the supplying of an AC motor through an adjustable speed drive by a PV / battery system, can operate with a better power quality.

ACKNOWLEDGMENT

The authors would like to acknowledge the French Republic, who through the scholarship program of the Service of Cooperation and Cultural Action (SCAC) of his Embassy in Cameroon, allowed us to spend 12 months of training at the Laboratory for Solar Energy and Energy Saving (LESEE), International Institute for Water and Environmental Engineering, 2iE-Ouagadougou - Burkina Faso. Our gratitude goes also to the General Director of 2iE who kindly welcomed us at 2iE. We would like to thank all the members of the LESEE, especially Mr. Henri KOTTIN, Mr. Moussa KADRI, Mr. Jacques KONANE and the student Mr. Kamal MASSARI who accompanied us during our experiments.

REFERENCES:

[1] M. Taylor and E.S. young, “Solar PV in Africa: costs and markets,” International Renewable Energy Agency (IRENA), 2016.

[2] R. Kempener, O.L. d’Ortigue, D. Saygin, J. Skeer, S. Vinci, and D. Gielen, “Off-grid renewable energy systems: status and methodological issues,” International Renewable Energy Agency (IRENA), 2015.

[3] IEA, “WEO - Energy access database,” 2018. [Online]. Available: http://www.worldenergyoutlook.org/resources/energydevelopment/energyaccessdatabase/. [Accessed: 19-Jan-2018].

[4] J. Guzinski, H. Abu-Rub, and P. Strankowski, Variable speed AC drives with inverter output filters. John Wiley & Sons, 2015, pp. 1-6.

[5] T. Wildi and G. Sybille, Electrotechnique, 4th ed. France: De Boeck, 2005, pp. 524-570.

[6] U. Sharma, S. Dwivedi, C. Jain and B. Singh, “Single Stage Solar PV Array Fed Field Oriented Controlled Induction Motor Drive for Water Pump,” in National Power Electronics Conference (NPEC), IIT Bombay, 2015.

[7] L. Zarour, R. Chenni, A. Borni and A. Bouzid, “Improvement of synchronous and asynchronous motor drive systems supplied by photovoltaic arrays with frequency control,” Journal of Electrical Engineering, vol. 59, no. 4, pp. 169–177, 2008.

[8] R. Saidur, S. Mekhilef, M.B. Ali, A. Safari, and H. A. Mohammed, “Applications of variable speed drive (VSD) in electrical motors energy savings,” Renewable and Sustainable Energy Reviews, vol. 16, no. 1, pp. 543–550, 2012.

[9] R. Saidur and T.M.I. Mahlia, “Energy, economic and environmental benefits of using high-efficiency motors to replace standard motors for the Malaysian industries,” Energy Policy, vol. 38, no. 8, pp. 4617–4625, Aug. 2010.

[10] F. Blaabjerg, H. Wang, P. Davari, X. Qu, and F. Zare, “Energy saving and efficient energy use by power electronic systems,” in Energy Harvesting and Energy Efficiency, N. Bizon, N. M. Tabatabaei, F. Blaabjerg, and E. Kurt Eds, Springer, 2017, pp. 1–14.

[11] R. Saidur, N.A. Rahim, H.W. Ping, M.I. Jahirul, S. Mekhilef, H.H. Masjuki, “Energy and emission analysis for industrial motors in Malaysia,” Energy Policy, vol. 37, no. 9, pp. 3650–3658, Sep. 2009.

[12] R. Saidur, N.A. Rahim, and M. Hasanuzzaman, “A review on compressed-air energy use and energy savings,” Renewable and Sustainable Energy Reviews, vol. 14, no. 4, pp. 1135–1153, 2010.

[13] T. Aziz, M. Ahmed, and Nahid-Al-Masood, “Investigation of harmonic distortions in photovoltaic integrated industrial microgrid,” Journal of Renewable and Sustainable Energy, vol. 10, no. 5, p. 053507, 2018.

[14] I. F II, “IEEE recommended practices and requirements for harmonic control in electrical power systems,” The Institute of Electrical and Electronics Engineers, p. 101, 1993.

[15] S. Nema, R.K. Nema, and G. Agnihotri, "Inverter topologies and control structure in photovoltaic applications: A review," Journal of Renewable and Sustainable Energy, vol. 3, no. 1, p. 012701, 2011.

[16] G. M. Shafiullah, A.M.T. Oo, A.B.M.S. Ali, P. Wolfs, and A. Stojcevski, "Experimental and simulation study of the impact of increased photovoltaic integration with the grid," Journal of Renewable and Sustainable Energy, vol. 6, no. 3, p. 033144, 2014.

[17] P. K. Bhatt and S.Y. Kumar, "Comprehensive Assessment and Mitigation of Harmonic Resonance in Smart Distribution Grid with Solar Photovoltaic," International Journal of Renewable Energy Research, vol. 7, no. 3, pp. 1085–1096, 2017.

[18] M. Khatri and A. Kumar, "Experimental Investigation of Harmonics in a Grid-Tied Solar Photovoltaic System," International Journal of Renewable Energy Research, vol. 7, no. 2, pp. 901–907, 2017.

[19] BIT, "Production de farine de maïs à petite echelle," BIT, Génève, ILO, WEP, Dossier technique 7, 1990, pp. 51-69.

[20] CIRAD, "Moulin à meules / Technologie post-récolte / Plateaux techniques - Plateforme technologie agroalimentaire - UMR Qualisud," 2012. [Online]. Available: https://plateforme-technologie-agroalimentaire.cirad.fr/plateaux-techniques/technologie-post-recolte/moulin-a-meules. [Accessed: 24-Apr-2018].

[21] CIRAD, "Broyeur à marteaux / Technologie post-récolte / Plateaux techniques - Plateforme technologie agroalimentaire - UMR Qualisud," 2012. [Online]. Available: https://plateforme-technologie-agroalimentaire.cirad.fr/plateaux-techniques/technologie-post-recolte/broyeur-a-marteaux. [Accessed: 24-Apr-2018].

[22] H. Haberlin, Photovotaic System Design and Practice. UK: John Wiley and Sons, ISBN, 2012, pp. 223-259.

[23] SMA, "Onduleur en îlotage SUNNY ISLAND 5048: Description technique." SMA Solar Technology AG, 2004.

[24] Studer Innotec, "Manuel utilisateur série Xtender: Appareil combiné onduleur, chargeur de batterie et système de transfert." Studer Innotec SA, V4. .0-2015.

[25] A. Chauvin, "Analyseur de réseaux électriques triphasés, C.A8335, QUALISTAR+. Notice de fonctionnement." Chauvin Arnoux Group, 2010.

[26] R. Langella, A. Testa, and A. Et, "IEEE Recommended Practice and Requirements for Harmonic Control in Electric Power Systems," The Institute of Electrical and Electronics Engineers, 2014.

[27] M. Azab and M.A. Awadallah, "Selective harmonic elimination in VSI-fed induction motor drives using swarm and genetic optimisation," International Journal of Power Electronic, vol. 5, no. 1, pp. 56–74, 2013.

[28] R. Sridhar, S. Dhar, and S.S. Dash, "Performance analysis of a stand alone PV system with reduced switch cascaded multilevel inverter," International Journal of Power and Energy Conversion, vol. 6, no. 2, pp. 107–127, 2015.

[29] D. Gallo, C. Landi, M. Luiso, and E. Fiorucci, "Analysis of a photovoltaic system: AC and DC power quality," WSEAS Transactions on Power Systems, vol. 8, no. 4, pp. 45–55, 2013.

[30] M.V. Aware and V.B. Virulkar, "Comparative performance of BESS and SMES in distribution network to improve power quality," International Journal of Power and Energy Conversion, vol. 1, no. 4, pp. 327–347, 2009.

[31] R. Dharmalingam, S.S. Dash, K. Senthilnathan, A.B. Mayilvaganan, and S. Chinnamuthu, "Power quality improvement by unified power quality conditioner based on CSC topology using synchronous reference frame theory," The Scientific World Journal, vol. 2014, Article ID 391975, 2014.

[32] P. Prabhakar and H. Vennila, "Power quality improvement in microgrid using custom power devices," International Journal of Enterprise Network Management, vol. 8, no. 4, pp. 327–339, 2017.